0022-3565/06/3172-546–552
THE JOURNAL OF PHARMACOLOGY AND EXPERIMENTAL THERAPEUTICS

JPET 317:546–552, 2006

Vol. 317, No. 2
96891/3112887
Printed in U.S.A.

Actions of a Histone Deacetylase Inhibitor NSC3852 (5-Nitroso-8-quinolinol) Link Reactive Oxygen Species to Cell Differentiation and Apoptosis in MCF-7 Human Mammary Tumor Cells

Anna Martirosyan, Stephen Leonard, Xianglin Shi, Brian Griffith, Peter Gannett, and Jeannine Strobl

Department of Biochemistry & Molecular Pharmacology (A.M., B.G., J.S.), Basic Pharmaceutical Sciences (P.G.), West Virginia University, Morgantown, West Virginia; Pathology & Physiology Research Branch, Health Effects Laboratory Division, National Institute for Occupational Safety and Health, Morgantown, West Virginia (S.L., X.S.); and Biomedical Sciences, Edward Via Virginia College of Osteopathic Medicine and Biomedical Sciences & Pathobiology, Virginia Polytechnic Institute & State University, Blacksburg, Virginia (J.S.)

Received October 16, 2005; accepted February 22, 2006

ABSTRACT

NSC3852 (5-nitroso-8-quinolinol) has cell differentiation and antiproliferative activity in human breast cancer cells in tissue culture and antitumor activity in mice bearing P388 and L1210 leukemic cells. We investigated the mechanism of NSC3852 action in MCF-7 human breast cancer cells using electron spin resonance (ESR). Reactive oxygen species (ROS) were detected in MCF-7 cell suspensions incubated with NSC3852 using the spin trap 5,5-dimethyl-1-pyrroline-*N*-oxide (DMPO). Formation of the DMPO-OH adduct was quenched by the addition of superoxide dismutase but not by catalase, and we concluded that superoxide was generated in the NSC3852-treated cells. The flavoprotein inhibitor diphenylene iodonium suppressed ROS production, providing evidence for the involvement of a flavin-dependent enzyme system in the ROS response to NSC3852. A biologically significant oxidative response to NSC3852 occurred in MCF-7 cells. An early marker of oxidative stress was a decrease in the [glutathione]/[glutathione disulfide] ratio 1 h after NSC3852 addition. Oxidative DNA damage, marked by the presence of 8-oxoguanine, and DNA-strand breakage occurred in cells exposed to NSC3852 for 24 h. Apoptosis peaked 48 h after exposure to NSC3852. Pretreatment with the glutathione precursor *N*-acetyl-L-cysteine (NAC) prevented DNA-strand breakage and apoptosis. Pretreatment with NAC also reversed NSC3852 decreases in E2F1, Myc, and phosphorylated retinoblastoma protein, indicative of redox-sensitive pathway(s) in MCF-7 cells during G_1 phase of the cell cycle. We conclude that ROS formation is involved in the apoptotic and cell differentiation responses to NSC3852 in MCF-7 cells.

Differentiation agents are promising experimental antitumor agents that modify epigenetic pathways in tumor cells (Mei et al., 2004; Piekarz and Bates, 2004; Somech et al., 2004). Differentiation agents cause growth arrest and expression of proteins typical of the normal cell phenotype in cancer cells, but these are transient effects (Munster et al., 2001a,b; Wang et al., 2001; Marks et al., 2004). The ability to trigger apoptosis in tumor cells is critical to the antitumor activity of differentiation agents; the mechanisms leading to

This work was funded by DAMD 17-00-1-500.

Portions of this work were presented in abstract form: Strobl J, Martirosyan A, Rahim-Bata R, Freeman A, and Clarke C (2004). Experimental breast cancer differentiation agents NSC3852, NSC69603, NSC10010, and NSC305819, in *1st ISC International Conference on Cancer Therapeutics, Molecular Targets, Pharmacology and Clinical Applications*; 2004 February 19–24, International Society of Chemotherapy and Società Italiana di Chemioterapia, Florence, Italy.

Article, publication date, and citation information can be found at http://jpet.aspetjournals.org.

doi:10.1124/jpet.105.096891.

ABBREVIATIONS: NSC3852, 5-nitroso-8-quinolinol; DMPO, 5, 5-dimethyl-1-pyrroline-*N*-oxide; DPI, diphenylene iodonium; DTNB, 5′,5-dithiobis-2-nitrobenzoic acid; DMEM, Dulbecco's modified Eagle's medium; ESR, electron spin resonance; GSH, glutathione; GSSG, glutathione disulfide; HDI, histone deacetylase inhibitor(s); MS-275, *N*-(2-aminophenyl)-4-[*N*-pyridin-3-yl-methoxycarbonyl)aminomethyl]benzamide; MTS, (3-(4, 5-dimethylthiazol-2-yl)-5-(3-carboxymethoxyphenyl) 2-(4-sulfonphenyl)-2*H*-tetrazolium; PBS, phosphate-buffered saline, pH 7.4; NAC, *N*-acetyl-L-cysteine; NSC2039, 8-quinolinol; Rb, retinoblastoma protein; ROS, reactive oxygen species; SAHA, suberoylanilide hydroxamic acid; SBHA, suberic bishydroxamate; SOD, superoxide dismutase; TSA, trichostatin A, [*R*-(*E*,*E*)]-7-[4-(dimethylamino)phenyl]-*N*-hydroxy-4,6-dimethyl-7-oxo-2,4-heptadienamide; FBS, fetal bovine serum.

tumor apoptosis vary with the individual differentiation agent and tissue type (Marks et al., 2000; Roy et al., 2005; Ungerstedt et al., 2005). We investigated the mechanism of the cell death and differentiation in human breast tumor cells exposed to a new antitumor agent, NSC3852 (5-nitroso-8-quinolinol).

A large number of inhibitors of class I/II histone deacetylases are now characterized, and we know that a variety of chemical structures possess histone deacetylase inhibitory activity (Fig. 1). The main classes of histone deacetylase inhibitor(s) (HDI) are 1) short-chain fatty acids, 2) hydroxamic acids, 3) cyclic tetrapeptides with and without amino-epoxy-oxodecanoic acid residues, and 4) benzamides. The hydroxamic acids, represented by suberoylanilide hydroxamic acid (SAHA) and trichostatin A (TSA), are among the most potent HDI. NSC3852 is a less potent HDI than SAHA, but has many similar effects in MCF-7 cells. Both cause growth arrest and accumulation of cells in G_0 phase of the cell cycle, as well as morphologic changes, such as formation of cytoplasmic lipid droplets and an enlargement of the cytoplasm (Munster et al., 2001b; Martirosyan et al., 2004). All HDI now appear to bind the zinc ion at the enzyme active site. NSC3852 lacks the hydroxamic acid moiety that is responsible for SAHA binding to Zn^{2+} in the histone deacetylase active site. NSC3852 harbors a different Zn^{2+} chelation motif, 8-quinolinol (Peters et al., 1974). We postulated that NSC3852 might exhibit novel actions in MCF-7 cells, because the quinoline ring and the nitroso substituent place NSC3852 in a chemically unique category of HDI. Our studies revealed that NSC3852, SAHA, and TSA stimulated ROS formation in MCF-7 cells and that NSC3852-induced oxidative stress contributed to apoptosis and differentiation in MCF-7 cells.

Materials and Methods

Tissue Culture. The MCF-7 human breast cancer cells (passage 40–55) were maintained in Dulbecco's modified Eagle's medium (DMEM) (BioWhittaker, Walkersville, MD) supplemented with 10% heat-inactivated fetal bovine serum (FBS), 2 mM glutamine, and 40 μg/ml gentamicin at 37°C in a humidified atmosphere of 6% CO_2/94% air. Cells were passaged every 4 to 5 days. Experiments were carried out in DMEM supplemented with 5% FBS. Cells were counted using a hemocytometer and 0.02% trypan blue to assess cell viability.

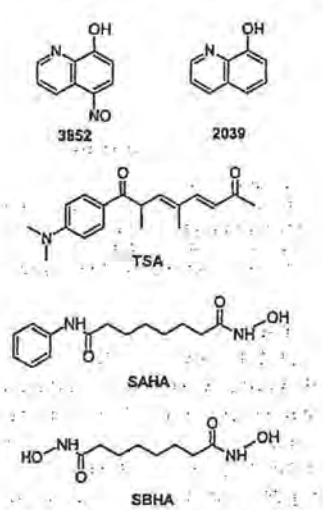

Fig. 1. Structures of NSC3852 and NSC2039 and other HDI.

Chemicals. NSC3852 and NSC2039 (8-quinolinol) were kindly provided by Dr. Robert Schultz (Drug Synthesis and Chemistry Branch, Developmental Therapeutics Program, Division of Cancer Treatment and Diagnosis, National Cancer Institute, Bethesda, MD). In this study, we used concentrations of NSC3852 and NSC2039 that inhibited proliferation of MCF-7 cells by 50% in a MTS cell proliferation assay (Martirosyan et al., 2004). TSA was from Upstate Biotechnology (Lake Placid, NY). SAHA and suberic bishydroxamate (SBHA) were gifts from Dr. Q. Zhou (Johns Hopkins University, Baltimore, MD). *N*-Acetyl-L-cysteine (NAC) and N^G-nitro-L-arginine methyl ester were from Sigma-Aldrich (St. Louis, MO). Dihydroethidium and 2′,7′-dihydrodichlorofluorescein diacetate were purchased from Molecular Probes (Eugene, OR).

Western Blot Analyses. Cells (2×10^6/60 mm^2) were treated 12 h after plating. Cells were harvested by scraping in 100°C lysis buffer (1% SDS and 10 mM Tris, pH 7.4) and heated (100°C, 5 min), and extracts were prepared by centrifugation in a microcentrifuge (4°C, 5 min). Protein concentrations were determined in aliquots of these extracts using the bicinchoninic acid assay (Pierce, Rockford, IL). Dithiothreitol (1 mM) and protease inhibitors were added [phenylmethylsulfonyl fluoride (1 mM), aprotinin (1 μg/ml), and leupeptin (1 μg/ml)] to the extracts. Protein samples (60–70 μg) were electrophoresed on 10% polyacrylamide gels and transferred to polyvinylidene difluoride membranes (Invitrogen, Carlsbad, CA). Membrane blocking and incubations with primary and secondary antibodies were performed as described previously (Zhou et al., 2002). Chemiluminescent signals were recorded on X-ray film and quantified using FluorChem (Alpha Innotech, San Leandro, CA) spot densitometry program with automatic background subtraction.

Free Radical Measurements. All ESR measurements were conducted using a Bruker EMX spectrometer (Bruker Instruments Inc., Billerica, MA) and a flat-cell assembly. Hyperfine couplings were measured (to 0.1 G) directly from magnetic field separation using potassium tetraperoxochromate (K_3CrO_8) and 1,1-diphenyl-2-picrylhydrazyl as reference standards (Janzen and Blackburn, 1968). The relative radical concentration was estimated by multiplying half of the peak height by $(\Delta H_{pp})^2$, where ΔH_{pp} represents peak-to-peak width. The Acquisit program was used for data acquisitions and analyses. MCF-7 cells (2.0×10^6 cells/60-mm^2 dish) were harvested 48 h after plating by trypsinization and collected at room temperature by centrifugation (225*g*, 5 min). Cells were washed once with ice-cold PBS and resuspended in ice-cold PBS at 2×10^6 cells/ml. Radical production was measured in the presence of the spin trap 5,5-dimethyl-1-pyrroline-*N*-oxide (DMPO; Aldrich Chemical Co., Milwaukee, WI). DMPO (200 mM) and 1×10^6 cells ± test agents were mixed in 1.0 ml of PBS, incubated at 37°C for 5 min, and then transferred to a flat cell for ESR measurements.

Intracellular Reactive Oxygen Species Detection. Cells were plated (2×10^6/35-mm^2 dish) in 3 ml of DMEM/5% FBS culture medium. After 12 h, cells were exposed to solvent control or 10 μM NSC3852. After the treatment, cells were exposed to 5 μM 2′,7′-dihydrodichlorofluorescein diacetate or dihydroethidium for 30 min. Cells were washed twice with PBS, and fluorescence was analyzed (10,000 events) using a FACScalibur flow cytometry (Becton Dickinson, San Jose, CA). Alternatively, cells plated onto sterile glass coverslips were fixed in 10% formaldehyde and examined using fluorescent confocal microscopy (Zeiss LSM 510).

Colorimetric Determination of Reduced and Oxidized Glutathione. The GSH and GSSG concentrations in MCF-7 cells (3×10^6cells/60-mm^2 dish) were measured enzymatically using the GSH/GSSG-412 kit (Oxis Research, Portland, OR). GSSG and GSH standards were prepared in 5% metaphosphoric acid. Cell samples were prepared in 5% metaphosphoric acid with or without 1-methyl-2-vinyl-pyridium trifluoromethane sulfonate, a GSH-specific scavenger. Ellman's reagent (5′,5-dithiobis-2-nitrobenzoic acid) reacts with

GSH to form a product with an absorption maximum at 412 nm. GSSG was determined using glutathione reductase to reduce GSSG to GSH followed by reaction with Ellman's reagent.

Comet Analysis. The comet assay is a single-cell gel electrophoresis method for measuring DNA damage. MCF-7 cells (2×10^5/35-mm^2 dish) were treated 12 h after plating. Twenty-four hours later, the cells were harvested and resuspended (1.5×10^5 cells/ml) in ice-cold PBS. The PBS cell suspension (50 μl) was mixed with 500 μl of 42°C low-melting point agarose, spread evenly (75 μl) onto a Comet Slide (Trevigen, Gaithersburg, MD), and allowed to harden. The slides were then immersed in ice-cold lysis solution (Trevigen) for 45 min to lyse the cells and then transferred to freshly prepared alkali solution (300 mM NaOH and 1 mM EDTA, pH 8.0) for 45 min at room temperature to denature the DNA. Electrophoresis was performed at 4°C. Slides were air-dried overnight at room temperature and then stained with SYBR Green (Trevigen). Comets were visualized by fluorescence microscopy at 630× magnification with the aid of an antifade solution. Comet images were analyzed using the LAI Automated Comet Assay Analysis System (Loats Associates, Inc., Westminster, MD). DNA damage was quantified in 80 comets per treatment/experiment using the tail moment [Tail moment = [(%DNA) (distance traveled)]].

Detection of Oxidative Damage to DNA. Oxidative damage to DNA was determined using the OxyDNA assay (Biotrin, Dublin, Ireland). MCF-7 cells were plated onto sterile glass coverslips in 35-mm^2 tissue culture dishes and treated with NSC3852 12 h later. After 24 h, cells were fixed and permeabilized with 99% methanol. Nonspecific binding sites were blocked using blocking solution (1 h, room temperature). After washing twice, the cells were incubated in the dark with fluorescein isothiocyanate-conjugated antibody (1 h, room temperature) to identify 8-oxoguanine containing DNA. Cell images were captured using confocal microscopy.

Cell Death Enzyme-Linked Immunosorbent Assay. We quantified cytoplasmic nucleosomes using the Cell Death Detection ELISA^{PLUS} kit (Roche Molecular Biochemicals, Indianapolis, IN) in MCF-7 cells plated in triplicate into 96-well plates. The cytoplasmic fractions from attached cells in each well were assayed in duplicate for the presence of nucleosomes according to the directions from the suppliers. The apoptotic response was measured by the nucleosome-enrichment fraction calculated as the ratio of the absorbance (405 nm) of drug-treated cultures/solvent-exposed cultures.

Statistics. Sigma plot software (SPSS Inc., Chicago, IL), version 5.0, and Prism (GraphPad Software, Inc., San Diego, CA), version 3.0, were used for statistical analysis. Statistically significant differences ($P < 0.05$) were determined using Student's t test or a one-way ANOVA and Tukey's t test ($P < 0.01$).

Results

Free Radical Generation in MCF-7 Cells Mediated by NSC3852. The structures of NSC3852 and NSC2039 appear in Fig. 1. NSC2039 is a control in our experiments, because it lacks the cell differentiation and histone deacetylase inhibitory activities of NSC3852 (Martirosyan et al., 2004).

We used ESR to examine ROS formation in MCF-7 cell suspensions. Figure 2 shows the ESR signals obtained with MCF-7 cell suspensions containing 10 μM NSC3852 or 8 μM NSC2039. In cells exposed to NSC3852, a 1:2:2:1 quartet signal (with $a_H = a_N = 14.9$ G, where a_H and a_N denote hyperfine splitting of the α-hydrogen and the nitroxyl nitrogen, respectively), indicative of the DMPO-OH adduct, was observed. In MCF-7 cells treated with NSC2039, no signal was produced demonstrating that the nitroso substituent was required for the generation of ROS (Fig. 2, scans A and B). Figure 3A shows the concentration-response relationship between the ESR-peak height in

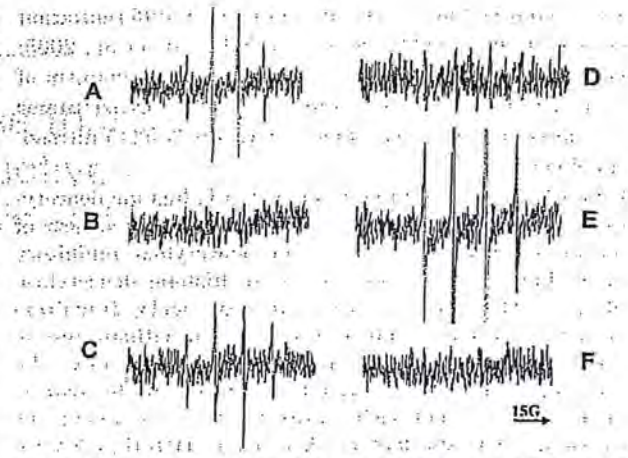

Fig. 2. ESR studies of NSC3852 and NSC2039 in MCF-7 cells. ESR spectra of MCF-7 cells (treated as indicated for 5 min, 37°C) were recorded with the spin trap DMPO (200 mM) in a 1×10^6 cell suspension in PBS. (A) NSC3852 (10 μM). (B) NSC2039 (8 μM). (C) NSC3852 (10 μM) + catalase (2000 U/ml). (D) NSC3852 + SOD (200 U/ml). (E) NSC3852 (10 μM) + rotenone (50 μM). (F) NSC3852 (10 μM) + DPI (20 μM). The ESR spectrometer settings were as follows: receiver gain, 6.32×10^4; time constant, 4 ms; modulation amplitude, 1.0 Gauss (G); scan time, 41 s; number of scans, 3; and magnetic field, 3480 ± 100 G. $n = 3$.

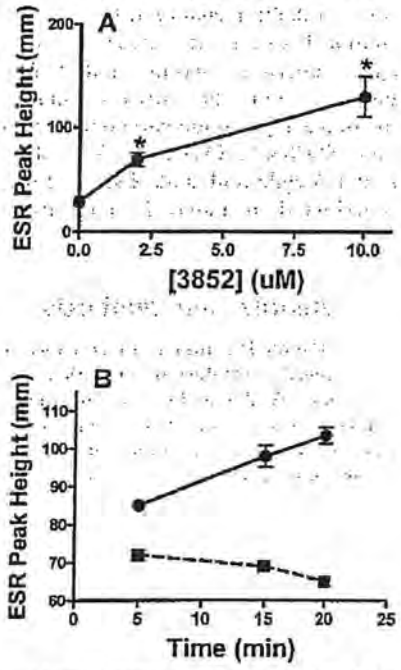

Fig. 3. A, concentration-response relationship for ROS production in MCF-7 cells exposed to NSC3852. Statistically significant ($P < 0.01$) ESR peak-height differences from controls are indicated (*). B, time course of ROS production in MCF-7 cells + NSC3852. ESR spectra of 1×10^6 MCF-7 cells + NSC3852 + 200 mM DMPO in PBS.

MCF-7 cells exposed to dimethyl sulfoxide solvent alone, 2 μM NSC3852, and 10 μM NSC3852. Statistically significant DMPO-OH peaks were generated at both the 2 and 10 μM NSC3852 concentrations. Figure 3B compares the time course of the signal intensity of the DMPO-OH peak in cells treated with 2 or 10 μM NSC3852. The MCF-7 ROS response to 2 μM NSC3852 decayed more rapidly than response to 10 μM. In cells treated with 10 μM NSC3852,

ROS production was stable for as long as we measured the reaction (25 min). No ROS were detected when NSC3852 or NSC2039 was diluted into PBS without MCF-7 cells, suggesting that cellular metabolism is involved in the ROS response to NSC3852.

To probe the source of the DMPO-OH ESR signal, either superoxide dismutase (SOD) or catalase was added to cell suspensions. Catalase, a scavenger of H_2O_2, had no effect upon the signal (Fig. 2, scan C). Therefore, the source of the DMPO-OH signal was unlikely to be $OH^{\cdot}$ derived from H_2O_2. An alternate route for the formation of DMPO-OH is through the trapping of superoxide to form the unstable adduct, DMPO-OOH that quickly decomposes to DMPO-OH. When SOD was added to the cell suspensions, the ESR signal was quenched (Fig. 2, scan D), consistent with data showing that, when SOD clears the $O_2^{\cdot-}$ (superoxide) very quickly, trapping of the unstable DMPO-OOH intermediate is suppressed. These results support our conclusion that the observed ESR spectra were produced by the decomposition of the DMPO-OOH signal trapped from superoxide (Halliwell and Gutteridge, 1999).

The two major cellular sources for production of $O_2^{\cdot-}$ are flavoproteins in NADPH oxidase complexes and in the mitochondrial electron transport chain (Berridge and Tan, 2000; Jezek and Hlavata, 2005). Diphenyliodonium is a nonselective flavoprotein inhibitor affecting all of the flavin-dependent enzymes. Because DMPO can enter cells, the ESR spectra in Fig. 2 depict both intracellular and extracellular ROS. The ESR spectra showing suppression of the DMPO-OH signal upon the addition of the enzyme SOD to the cell suspension (Fig. 2D) suggested that at least half of the ESR signal was produced extracellularly. The nonphagocytic form of membrane NADPH oxidase, a flavin-dependent enzyme, is the most likely source of extracellular superoxide (Berridge and Tan, 2000).

We also demonstrated intracellular superoxide production in MCF-7 cells in response to 10 μM NSC3852 using the fluorescent probes dihydroethidium and 2′-7′-dihydrodichlorofluorescein diacetate (data not shown). The identity and relative contribution of the enzymes responsible for the intracellular ROS response of MCF-7 cells to NSC3852 are not fully established; however, the complete inhibition of the ESR signals with DPI (Fig. 2F) strongly implicated flavin-dependent enzymes, such as NADPH oxidase, the mitochondrial Complex I, nitric-oxide synthase, aromatase, and other cytochrome P450-dependent enzymes present in breast cancer (Karihtala et al., 2004; Dumitrescu and Cotarla, 2005). Using 1 mM N^G-nitro-L-arginine methyl ester to inhibit nitric-oxide synthase in MCF-7 cells, we showed a 29.5% ($P < 0.01$) reduction in the DMPO-OH ESR signal intensity, indicating that nitric-oxide synthase is important to the mechanism of action of NSC3852.

Augmentation of the NSC3852-generated DMPO-OH ESR signal by rotenone (Fig. 2E) is evidence for a role of mitochondrial Complex I in the intracellular ROS response to NSC3852. When rotenone binds Complex I, electron transport to ubiquinone is interrupted, resulting in superoxide formation (Majander et al., 1994; Jezek and Hlavata, 2005). Alternatively, there is evidence in brain microglia that rotenone can directly stimulate NADPH oxidase activity, thus enhancing the DMPO-OH signal intensity (Zoccarato et al., 2005). Thus, our data support a model in which NSC3852 stimulates ROS production through a variety of cellular-dependent pathways.

Regulation of G_1 Proteins by NSC3852 and Reversal by *N*-Acetyl-L-cysteine. Cell-cycle arrest in G_1 is a prerequisite for differentiation of human breast tumor cells in culture. Initial responses to differentiation stimuli include a shift in the expression of cell-cycle regulatory proteins toward their status in early G_1 phase of the cell cycle, specifically hypophosphorylated retinoblastoma protein (Rb), and decreases in E2F1 and Myc protein (Jensen et al., 2001; Munster et al., 2001; Wang et al., 2001). Earlier work showed that MCF-7 cells treated with NSC3852 accumulated in G_0 after 48 h but that MCF-7 cells exposed to the related analog, NSC2039, did not (Martirosyan et al., 2004). Based upon the differential ability of NSC3852 and NSC2039 to generate ROS and to cause differentiation in MCF-7 cells, we performed Western blot analyses of Rb, E2F1, and Myc.

NSC3852 caused a time-dependent accumulation of hypophosphorylated Rb and loss of phosphorylated Rb between 12 and 48 h. There were no detectable differences in Rb between control and NSC3852-treated cells at 8 h or earlier. Statistically significant decreases in phosphorylated Rb and E2F1 protein levels were seen at 12 and 24 h. After 24 h, Myc protein levels had decreased significantly, and by 48 h, Myc was undetectable in the Western blots. The time-dependent shift in the profile of Rb, E2F1, and Myc expression is consistent with the progression of NSC3852-treated cells into G_0 (Martirosyan et al., 2004).

Figure 4 compares the effects of NSC3852 and NSC2039 on the G_1 protein profile at 24 h. There were no statistically significant differences in Rb, E2F1, or Myc protein levels between control and NSC2039-treated cells. In NSC3852-treated cells, E2F1 and Myc levels fell by 50% ($n = 3$, $p < 0.05$), and hypophosphorylated Rb levels increased significantly. Figure 4 also shows the dependence upon a NAC-sensitive pathway for the NSC3852-mediated shift in Rb, E2F1, and Myc protein expression. Cells pretreated with 5 mM NAC 1 h before the addition of NSC3852 displayed no significant changes in Rb phosphorylation state, E2F1, and Myc. The effect of NAC pretreatment suggested that a redox-sensitive mechanism in G_1 phase might be involved in the actions of NSC3852.

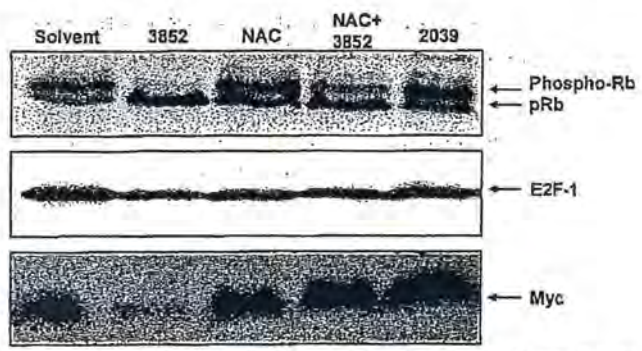

Fig. 4. Actions on the Rb/E2F-1/Myc pathway. Synchronized MCF-7 cells (2×10^6) were plated in 60-mm^2 dishes in 5 ml of DMEM/5% FBS. Twelve hours later, 5 mM NAC or water was added for 1 h as indicated. NSC3852 (10 μM) or NSC2039 (8 μM) then was added for 24 h. Cells were harvested for Western blot analysis. Proteins (80 μg/lane) were resolved on 10% polyacrylamide gels, and blots were probed with polyclonal antibodies to phospho-Rb and hypophosphorylated Rb (pRb), E2F1, and Myc.

NSC3852 Effect on [GSH]/[GSSG] Ratio in MCF-7 Cells. The major redox couple in mammalian cells is GSH-GSSG, and decreases in the intracellular [GSH]/[GSSG] ratio are a biological indicator of oxidative stress. NSC3852 stimulated O_2 levels within 15 min sufficiently to raise intracellular [GSSG] and thereby decrease the [GSH]/[GSSG] ratio. After 1 h, NSC3852 decreased the [GSH]/[GSSG] by 20% compared with control cells ($P < 0.05$). By 6 h, the [GSH]/[GSSG] ratios in control and treated cells were statistically indistinguishable, suggesting that NSC3852 mediated a transient oxidative shift in the cellular redox potential.

Free Radical Generation in MCF-7 Cells by Histone Deacetylase Inhibitors. NSC3852 is not unique among tumor differentiation agents in eliciting ROS. Three additional HDI (TSA, SAHA, and SBHA) elicited rapid and robust ESR signals indicative of ROS production in MCF-7 cells. The relative peak heights of the ESR signals (mean ± range, $n = 2$) were measured in parallel aliquots of 1×10^6 MCF-7 cells treated with 200 nM TSA (99 ± 1 mm), 200 nM SAHA (98 mm), 10 μM 3852 (109 ± 3 mm), or 2 μM 3852 (70 ± 4 mm) for 5 min at 37°C. We conclude that the magnitude of the ROS signals produced by these concentrations of HDI is roughly equivalent (Fig. 5). Previous work using a ROS-sensitive fluorescence dye showed that SAHA and another HDI, MS-275, increased ROS production in human leukemia cells (Rosato et al., 2003; Rahmani et al., 2005). This report is the first to demonstrate ROS generation in response to HDI using ESR.

DNA Damage and Apoptotic Effects of NSC3852 in MCF-7 Cells. ROS and oxidative stress produce DNA damage that can trigger apoptosis (Guetens et al., 2002). We performed comet assays to test for DNA damage by NSC3852 and measured the extent of damage as the increase in the comet tail moment. NSC3852-induced DNA damage was detected after 12 h and was maximal at 24 h. DNA damage was undetectable after 96 h (Fig. 6A), at which time an apoptotic response might have eliminated cells with damaged DNA. Therefore, after treatment with NSC3852, the cells behaved as if they were exposed to an oxidative stress that was either self-limiting or attenuated by compensatory cell-survival pathways.

Three lines of evidence support the role of ROS in the DNA-damage response. First, pretreatment with 5 mM NAC 1 h before NSC3852 prevented DNA damage as measured at the 24-h time point of peak damage (Fig. 6B). Second, NSC2039 did not induce DNA damage in MCF-7 cells (Fig. 6B). Third, we used immunohistochemistry to detect 8-oxoguanine, a DNA adduct formed during free radical damage to DNA. All cells in the NSC3852-treated group contained nuclear 8-oxoguanine after 24 h, whereas control cells stained very weakly for this adduct (Fig. 7).

Apoptosis occurred in response to NSC3852, and a 1-h pretreatment with NAC blocked this response (Fig. 8). The peak NSC3852 DNA-damage response occurred at 24 h (Fig. 6A) and preceded the peak in NSC3852-induced apoptosis (48 h) (Fig. 8). This temporal relationship fits a model where NSC3852-induced formation of 8-oxoguanine DNA adducts leads to DNA-strand breakage and apoptotic cell death.

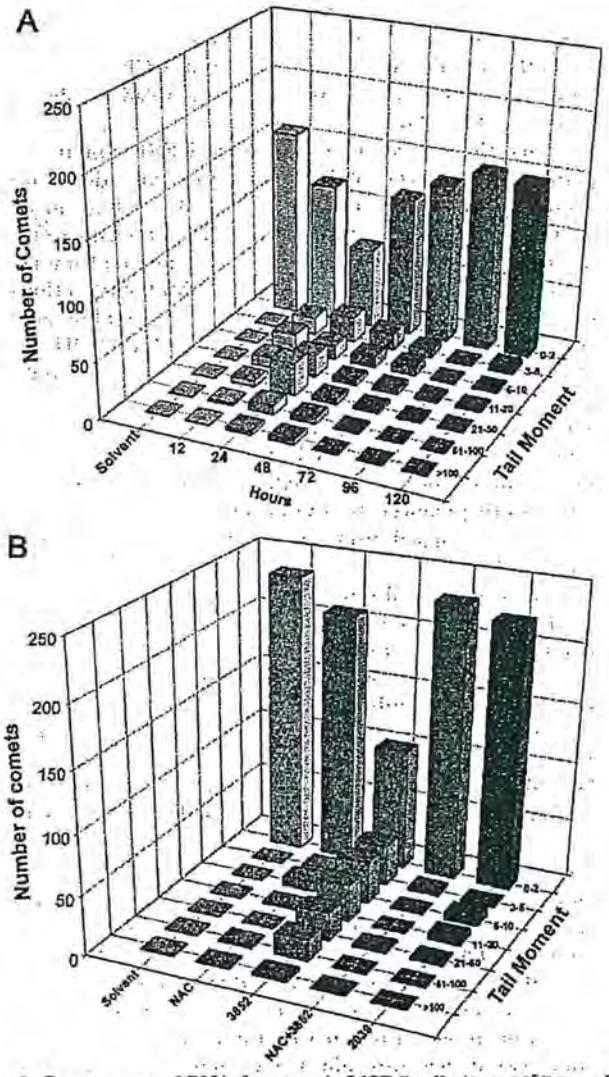

Fig. 6. Comet assay of DNA damage. A, MCF-7 cells (1×10^5/35-mm² dish) were plated, and 12 h later, a single application of NSC3852 to the medium (10 μM) or an equivalent amount of solvent (0.01% dimethyl sulfoxide) was delivered. Cells were harvested 12, 24, 48, 72, 96, and 120 h later and assayed for comets. Data shown are pooled results of two independent experiments of 80 comets each. B, MCF-7 cells (1×10^6/35-mm² dish) were treated with 10 μM NSC3852 or 8 μM NSC2039 for 24 h and then assayed for DNA damage. The numbers of comets with tail moments in ranges among zero to two, five to 10, 10 to 20, 20 to 50, 50 to 100, and >100 are plotted for each treatment group. Eighty cells were analyzed per experiment. Data shown are pooled results of the three independent comet experiments.

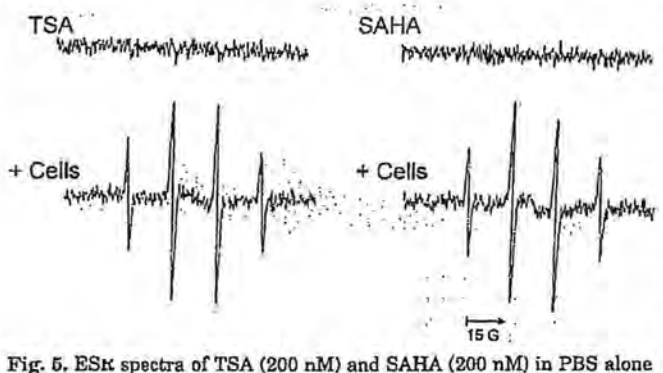

Fig. 5. ESR spectra of TSA (200 nM) and SAHA (200 nM) in PBS alone or after incubation with 1×10^6 MCF-7 cells (5 min, 37°C) as described in Fig. 2.

Fig. 7. Detection of 8-oxoguanine. MCF-7 cells (2×10^6) on sterile glass coverslips were treated 24 h with vehicle control or 10 μM NSC3852. 8-Oxoguanine was detected immunohistochemically.

Discussion

NSC3852 was recently identified as a breast cancer differentiation agent with histone deacetylase activity (Martirosyan et al., 2004). The purpose of this work was to understand the mechanistic basis for its pleiotropic actions in human breast cancer cells that are of potential significance in the treatment of cancer. One important finding was the enrichment of Rb in its hypophosphorylated state in NSC3852-treated cells. Hypophosphorylated Rb is the active tumor suppressor state of Rb and is a marker of cells arrested in G_1, cell differentiation, and cell senescence (Yen and Varvayanis, 1995; Knudsen et al., 1998; Yen et al., 2004). We also showed that NSC3852 is a redox-active compound that stimulates superoxide production and a transient rise in intracellular redox potential. Our studies demonstrated that ROS production is important to the mechanism of action of NSC3852. ROS generation is dependent upon the interaction of NSC3852 with the cells and occurs both intracellularly and extracellularly. We propose that ROS production has dual actions in MCF-7 cells stimulating apoptosis through a well established mechanism of oxidative DNA damage (Guetens et al., 2002) and promoting cell differentiation through its actions on Rb protein.

The basis for our hypothesis that NSC3852 acts on Rb phosphorylation status by a redox mechanism is the reversal of NSC3852 activity by *N*-acetyl-L-cysteine pretreatment and the failure of NSC2039, a non-ROS-generating analog, to change Rb status. The temporal series of events following treatment with NSC3852 suggest that a ROS-initiated cascade of events leads to hypophosphorylated Rb, but our data do not exclude a direct action of ROS upon Rb. Other investigators have also concluded that cellular redox status regulates the phosphorylation state of Rb (Dou et al., 1995; Nelson et al., 1997; Yamauchi and Bloom, 1997; Esposito et al., 2000; Kennedy et al., 2002).

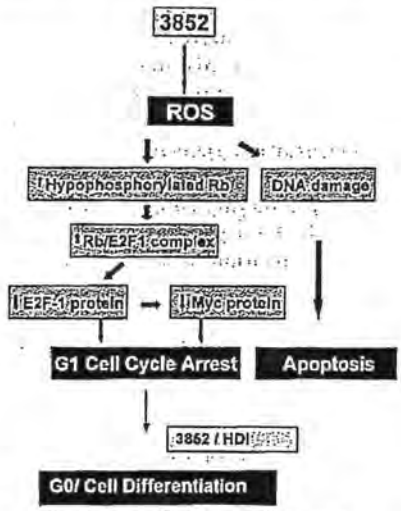

Fig. 9. Model of NSC3852 action.

The work of Cicchillitti et al. (2003) suggests that protein phosphatase 2A, the enzyme responsible for the dephosphorylation of Rb, responds to cellular redox status. These investigators showed that, as the intracellular redox potential rises in response to oxidative stress, phosphatase 2A activity is stimulated, increasing hypophosphorylated Rb. The idea that Rb acts as a thiol-dependent nanotransducer of intracellular redox state and cell-cycle progression/differentiation status is intriguing and is the foundation of a model of redox control of cell proliferation proposed by Hoffman et al. (2001). However, there is substantial support for the opposing hypothesis that oxidative stress is mitogenic and antioxidants suppress proliferation (Irani et al., 1997; Chueh, 2000; Menon et al., 2003). All thiol residues on proteins are redox-sensitive and theoretically transduce redox signals rapidly and reversibly via changes in protein structure. A broader examination of redox signaling in cell-cycle regulatory pathways is one approach to resolving this paradox (Li and Oberley, 1998; Moran et al., 2001; Cooper et al., 2002; Kern and Kehrer, 2005; Ungerstedt et al., 2005).

Our model describing a dual role for ROS in the cell differentiation and apoptotic responses to NSC3852 in MCF-7 cells appears in Fig. 9. We propose that a transient rise in intracellular redox potential establishes conditions permissive for differentiation to take place. Hypophosphorylated Rb will bind E2F and inhibit activation of genes, such as c-*myc*, that are required for progression through the cell cycle. Reductions in Myc protein reduce E2F transcription and syn-

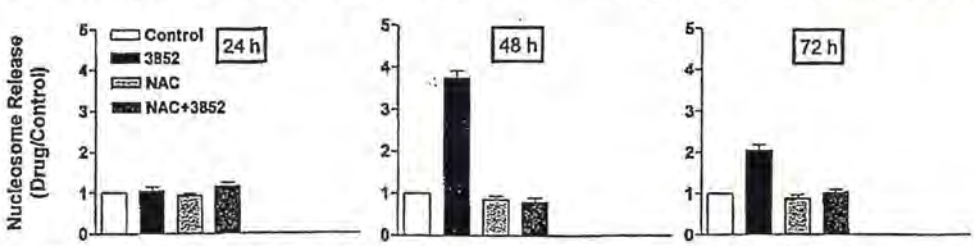

Fig. 8. Nucleosome-release apoptosis assay. MCF-7 cells (4000 per well) were plated in 96-well plates. Twelve hours later, cells were pretreated with NAC (as indicated); vehicle (control) or NSC3852 (10 μM) was added for 24, 48, or 72 h. Apoptosis was assayed using a nucleosome release enzyme-linked immunosorbent assay and is reported here as the ratio of treated/control values obtained in a single experiment performed in triplicate.

thesis. After a permissive state for differentiation exists, what additional stimuli activate the differentiation response? NSC3852 inhibits histone deacetylase activity in vitro at the same concentrations used in this study, and we suggest that inhibition of histone deacetylase is a requisite step in the differentiation response to NSC3852. Furthermore, because TSA, SAHA, and SBHA also generate ROS in MCF-7 cells, ROS production coupled with histone deacetylase inhibition might be a general mechanism for inducing apoptosis and differentiation in breast cancer.

Acknowledgments

We thank Drs. Andrew Shiemke and Diana Beattie for helpful comments on this manuscript.

References

Berridge MV and Tan AS (2000) Cell-surface NAD(P)H-oxidase: relationship to trans-plasma membrane NADH-oxidoreductase and a potential source of circulating NADH-oxidase. *Antioxid Redox Signal* 2:277–288.

Cicchillitti L, Fasanaro P, Biglioli P, Capogrossi MC, and Martelli F (2003) Oxidative stress induces protein phosphatase 2A-dependent dephosphorylation of the pocket proteins pRb, p107, and p130. *J Biol Chem* 278:19509–19517.

Chueh P-J (2000) Cell membrane redox systems and transformation. *Antioxid Redox Signal* 2:177–187.

Cooper CE, Patel RP, Brookes PS, and Darley-Usmar VM (2002) Nanotransducers in cellular redox signaling: modification of thiols by reactive oxygen and nitrogen species. *Trends Biochem Sci* 27:489–492.

Dou QP, An B, and Will PL (1995) Induction of a retinoblastoma phosphatase activity by anticancer drugs accompanies p53-independent G_1 arrest and apoptosis. *Proc Natl Acad Sci USA* 92:9019–9023.

Dumitrescu RG and Cotarla I (2005) Understanding breast cancer risk. . . where do we stand in 2005? *J Cell Mol Med* 9:208–221.

Esposito F, Russo L, Russo T, and Cimino F (2000) Retinoblastoma protein dephosphorylation is an early event of cellular response to prooxidant conditions. *FEBS Lett* 470:211–215.

Gustens G, De Boeck G, Highley M, van Oosterom AT, and de Bruijn EA (2002) Oxidative DNA damage: biological significance and methods of analysis. *Crit Rev Clin Lab Sci* 39:331–457.

Halliwell B and Gutteridge JMC (1999) *Free Radicals in Biology and Medicine*, 3rd Ed., Oxford University Press, NY.

Hoffman A, Spetner LM, and Burke M (2001) Cessation of cell proliferation by adjustment of cell redox potential. *J Theor Biol* 211:403–407.

Irani K, Xia Y, Zweier JL, Sollott SJ, Der CJ, Fearon ER, Sundaresan M, Finkel T, and Goldschmidt-Clermont PJ (1997) Mitogenic signaling mediated by oxidants in ras-transformed fibroblasts. *Science (Wash DC)* 275:1649–1652.

Janzen EG and Blackburn BJ (1968) Detection and identification of short-lived free radicals by an electron spin resonance trapping technique. *J Am Chem Soc* 90: 5909–5910.

Jensen SS, Madsen MW, Lukas J, Binderup L, and Bartek J (2001) Inhibitory effects of 1α,25-dihydroxyvitamin D3 on the G_1-S phase-controlling machinery. *Mol Endocrinol* 15:1370–1380.

Jezek P and Hlavata L (2005) Mitochondria in homeostasis of reactive oxygen species in cell, tissues, and organisms. *Int J Biochem Cell Biol* 37:2478–2503.

Karihtala P, Kinnula VL, and Soini Y (2004) Antioxidative response for nitric oxide production in breast carcinoma. *Oncol Rep* 12:755–759.

Kennedy DO, Kojima A, Moffatt J, Yamagiwa H, Yano Y, Hasuma T, Otani S, and Matsui-Yuasa I (2002) Cellular thiol status-dependent inhibition of tumor cell growth via modulation of retinoblastoma protein phosphorylation by (−)-epigallocatechin. *Cancer Lett* 179:25–32.

Kern JC and Kehrer JP (2005) Free radicals and apoptosis: relationships with glutathione, thioredoxin, and the BCL family of proteins. *Front Biosci* 10:1727–1738.

Knudsen ES, Buckmaster C, Chen TI, Feramisco JR, and Wang JY (1998) Inhibition of DNA synthesis by RB: effects on G_1/S transition and S-phase progression. *Genes Dev* 12:2278–2298.

Li N and Oberley TD (1998) Modulation of antioxidant enzymes, reactive oxygen species, and glutathione levels in manganese superoxide dismutase overexpressing NIH/3T3 fibroblasts during the cell cycle. *J Cell Physiol* 177:148–160.

Majander A, Finel M, and Wikstrom M (1994) Diphenylene iodonium inhibits reduction of iron-sulfur clusters in the mitochondrial NADH-ubiquinone oxidoreductase (Complex I). *J Biol Chem* 269:21037–21042.

Marks PA, Richon VM, Miller T, and Kelly WK (2004) Histone deacetylase inhibitors. *Adv Cancer Res* 91:137–168.

Marks PA, Richon VM, and Rifkind RA (2000) Histone deacetylase inhibitors: inducers of differentiation or apoptosis of transformed cells. *J Natl Cancer Inst* 92:1210–1216.

Martirosyan AR, Rahim-Bata R, Freeman AB, Clarke CD, Howard RL, and Strobl JS (2004) Differentiation-inducing quinolines as experimental breast cancer agents in the MCF-7 human breast cancer model. *Biochem Pharmacol* 68:1729–1738.

Mei S, Ho AD, and Mahlknecht U (2004) Role of histone deacetylase inhibitors in the treatment of cancer. *Int J Oncol* 25:1509–1519.

Menon SG, Sarsour EH, Spitz DR, Higashikubo R, Sturm M, Zhang H, and Goswami PC (2003) Redox regulation of the G_1 to S phase transition in the mouse embryo fibroblast cell cycle. *Cancer Res* 63:2109–2117.

Moran LK, Gutteridge JMC, and Quinlan GJ (2001) Thiols in cellular redox signaling and control. *Curr Med Chem* 8:763–772.

Munster PN, Srethapakdi M, Moasser MM, and Rosen N (2001a) Inhibition of heat shock protein 90 function by ansamycins causes the morphological and functional differentiation of breast cancer cells. *Cancer Res* 61:2945–2952.

Munster PN, Troso-Sandoval T, Rosen N, Rifkind R, Marks PA, and Richon VM (2001b) The histone deacetylase inhibitor suberoylanilide hydroxamic acid induces differentiation of human breast cancer cells. *Cancer Res* 61:8492–8497.

Nelson DA, Krucher NA, and Ludlow JW (1997) High molecular weight protein phosphatase type 1 dephosphorylates the retinoblastoma protein. *J Biol Chem* 272:4528–4535.

Peters DG, Hayes JM, and Hieftje GM (1974) *Theory and Practice of Analytical Chemistry*, WB Saunders Co., Philadelphia.

Piekarz R and Bates S (2004) A review of depsipeptide and other histone deacetylase inhibitors in clinical trials. *Curr Pharm Des* 10:2289–2298.

Rahmani M, Reese E, Dai Y, Bauer C, Payne SG, Dent P, Spiegel S, and Grant S (2005) Coadministration of histone deacetylase inhibitors and perifosine synergistically induces apoptosis in human leukemia cells through Akt and ERK1/2 inactivation and the generation of ceramide and reactive oxygen species. *Cancer Res* 65:2422–2432.

Rosato RR, Almenara JA, and Grant S (2003) The histone deacetylase inhibitor MS-275 promotes differentiation and apoptosis in human leukemic cells through a process regulated by generation of reactive oxygen species and induction of p21 CIP1/WAF1. *Cancer Res* 63:3637–3645.

Roy S, Packman K, Jeffrey R, and Tenniswood M (2005) Histone deacetylase inhibitors differentially stabilize acetylated p53 and induce cell cycle arrest or apoptosis in prostate cancer cells. *Cell Death Diff* 12:482–491.

Somech R, Izraeili A, and Simon AJ (2004) Histone deacetylase inhibitors—a new tool to treat cancer. *Cancer Treat Rev* 30:461–472.

Ungerstedt JS, Sowa Y, Xu W-S, Shao Y, Dokmanovic M, Perez G, Ngo L, Holmgren A, Jiang X, and Marks PA (2005) Role of thioredoxin in the response of normal and transformed cells to histone deacetylase inhibitors. *Proc Natl Acad Sci USA* 102:673–678.

Wang Q, Lee D, Sysounthone V, Chandraratna RAS, Christakos S, Korah R, and Wieder R (2001) 1,25-Dihydroxyvitamin D3 and retinoic acid analogues induce differentiation in breast cancer cells with function- and cell-specific additive effects. *Breast Cancer Res Treat* 67:157–168.

Yamauchi A and Bloom ET (1997) Control of cell cycle progression in human natural killer cells through redox regulation of expression and phosphorylation of retinoblastoma gene product protein. *Blood* 89:4092–4099.

Yen A, Fenning R, Chandraratna R, Walker P, and Varvayanis S (2004) A retinoic acid receptor β/γ-selective prodrug (tazarotene) plus a retinoic X receptor ligand induces extracellular signal-regulated kinase activation, retinoblastoma hypophosphorylation, G_0 arrest, and cell differentiation. *Mol Pharmacol* 66:1727–1737.

Yen A and Varvayanis S (1995) RB phosphorylation in sodium butyrate-resistant HL-60 cells: cross-resistance to retinoic acid but not vitamin D3. *J Cell Physiol* 163:502–509.

Zhou Q, McCracken MA, and Strobl JS (2002) Control of mammary tumor cell growth *in vitro* by novel cell differentiation and apoptosis agents. *Breast Cancer Res Treat* 75:107–117.

Zoccarato F, Toscano P, and Alexandre A (2005) Dopamine derived dominochrome promotes H_2O_2 release at mitochondrial complex I: stimulation by rotenone, control by Ca^{2+}, and relevance to Parkinson disease. *J Biol Chem* 280:15587–15594.

Address correspondence to: Dr. Jeannine S. Strobl, Edward Via Virginia College of Osteopathic Medicine, 2265 Kraft Drive, Blacksburg, VA 24060. E-mail jstrobl@vcom.vt.edu